COMMUNICATIONS IN COMPUTATIONAL PHYSICS
Vol. **5**, No. 2-4, pp. 730-744

Commun. Comput. Phys.
February 2009

Variable High Order Multiblock Overlapping Grid Methods for Mixed Steady and Unsteady Multiscale Viscous Flows

Björn Sjögreen[1,*] and H. C. Yee[2]

[1] *Center for Applied Scientific Computing, Lawrence Livermore National Laboratory, Livermore, CA 94551, USA.*
[2] *NASA Ames Research Center, Moffett Field, CA 94035, USA.*

Received 21 December 2007; Accepted (in revised version) 26 June 2008

Available online 1 August 2008

Abstract. Flows containing steady or nearly steady strong shocks on parts of the flow field, and unsteady turbulence with shocklets on other parts of the flow field are difficult to capture accurately and efficiently employing the same numerical scheme, even under the multiblock grid or adaptive grid refinement framework. While sixth-order or higher-order shock-capturing methods are appropriate for unsteady turbulence with shocklets, third-order or lower shock-capturing methods are more effective for strong steady or nearly steady shocks in terms of convergence. In order to minimize the short comings of low order and high order shock-capturing schemes for the subject flows, a multiblock overlapping grid with different types of spatial schemes and orders of accuracy on different blocks is proposed. The recently developed single block high order filter scheme in generalized geometries for Navier Stokes and magnetohydrodynamics systems is extended to multiblock overlapping grid geometries. The first stage in validating the high order overlapping approach with several test cases is included.

AMS subject classifications: 65Z05, 65M06, 65M50, 65M55, 65M60, 65M99, 65Y99

Key words: Multiblock grid, overset grids, high order numerical methods, blunt body hypersonic flows, mixed steady and unsteady flows.

1 Introduction

For over two decades, second and third-order shock-capturing schemes employing time-marching to the steady state have enjoyed much success in simulating many transonic,

*Corresponding author. *Email addresses:* `sjogreen2@llnl.gov` (B. Sjögreen), `helen.m.yee@nasa.gov` (H. C. Yee)

supersonic and hypersonic steady aeronautical flows containing strong shocks. Standard second and third-order shock-capturing schemes are formally of second or third order and can degenerate to first-order of accuracy at steep gradients and smooth extrema. In the presence of mixed steady and unsteady multiscale viscous flows, low order (third-order or lower) time-accurate methods are not effective in accurately simulating, e.g., unsteady turbulent fluctuation containing shocklets. At the same time, high order schemes with good unsteady shock-capturing capability suffer from the inability to converge to the proper steady shocks effectively. Attempts to improve the convergence rate of high order methods to strong steady shocks involve order reduction or added numerical dissipation of the scheme in the vicinity of the shocks, thus degrading the true order of the scheme in other parts of the flow. Although extreme grid refinement in conjunction with low order schemes can be used on the unsteady turbulence part of the flow field, increases in CPU time, and instability and stiffness of the overall computations are inevitable. A method to effectively overcome these difficulties for mixed steady and unsteady viscous flows is a multiblock overlapping grid with a different order and different type of numerical scheme on different blocks.

This work concentrates on the finite difference formulation on structured grids. In particular, the aim is to extend our recently developed single block high order filter scheme in generalized geometries [11] to multiblock overlapping grid geometries. Stable SBP (summation-by-parts) energy norm numerical boundary procedures [5] for high order central spatial schemes are employed at physical boundaries. Lagrangian interpolations are used to interpolate grid point values among the block overlapping regions [2]. Matching high order spatial schemes for viscous terms and high order 3-D metric evaluations [10] is used in the presence of physical viscosity and curvilinear grids, respectively. In other words, the metric derivatives of the coordinate transformation are approximated by the same high order finite difference operators as used for to approximate the flux derivatives. These wide high-order finite difference operators for the metric evaluations employ summation-by-parts boundary closure as well. The multiblock option can, e.g., easily accommodate low order shock-capturing schemes in regions of steady shocks and high order schemes in regions containing unsteady turbulence and shocklets.

The interpolation between grids is not conservative, however conservation is less important when solving equations with physical viscosity such as the Navier-Stokes equations. In practical computations with inviscid equations, conservation at interfaces is usually not needed. In some very special cases non-conservation can lead to problems, see [6] for a discussion of this and a description of a conservative interpolation algorithm.

The following presents a description of the approach with some test cases to validate the solver without all the relevant physics included in the model. This is the first step of the development to validate the approach if a smooth transition can be accomplished at multiblock interfaces. The work in progress next step is to apply the solver to practical applications.

An important application for the proposed solver is to simulate blunt body space vehicles at hypersonic speeds with strong steady or nearly steady bow shocks and possi-

ble complex turbulence/shocklet interaction near the shoulder of the space vehicles and wake region at different angles of attack. It is also important for the study of the leading edge heat shield due to surface irregularities and/or isolated surface singularities such as very small openings. Another application is in numerical modeling of the heliosphere, space weather forecastings, supernova explosions and inertial confinement fusion.

2 Overlapping grid hierarchies

Overlapping grids have a long history in computational fluid dynamics (CFD). One of the first overlapping grid systems was developed in [1]. For basic descriptions see [2]. Here, we review some of the key ingredients on overlapping grids and discuss the high order overlapping procedures.

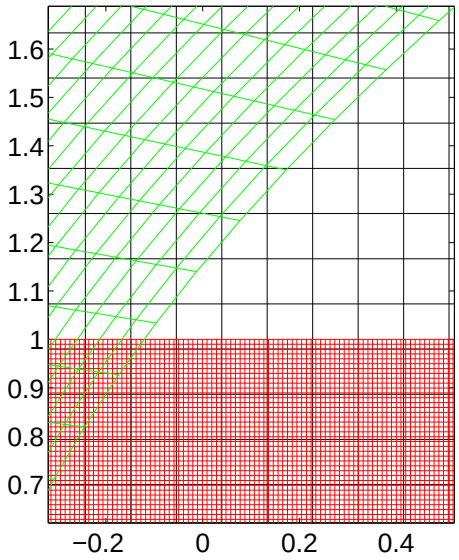

Figure 1: Three overlapping grids. The fine grid (red) and curvilinear grid (green) would be given higher priority than the coarse grid (black).

Fig. 1 shows a schematic of an overlapping grid system where three component grids meet. In regions of overlap, one grid carries the computed solution and parts of other grids in the same region are cut away. The grids are ordered in Fig. 1. The coarsest grid(black) would normally be given the lowest priority, and the parts of it that are covered by the fine grid (red) or the curvilinear grid (green) would be unused. The boundaries of the uncovered regions of the grids obtain values by interpolation from other grids. The interpolation is always two way. At the interface between two grids, say G_1 and G_2, the boundary of G_1 interpolates from G_2 and the boundary of G_2 interpolates from G_1. The interpolation can be implicit or explicit. In explicit interpolation, the points in G_2 that are used in the interpolation stencil for computing values at the boundary of G_1

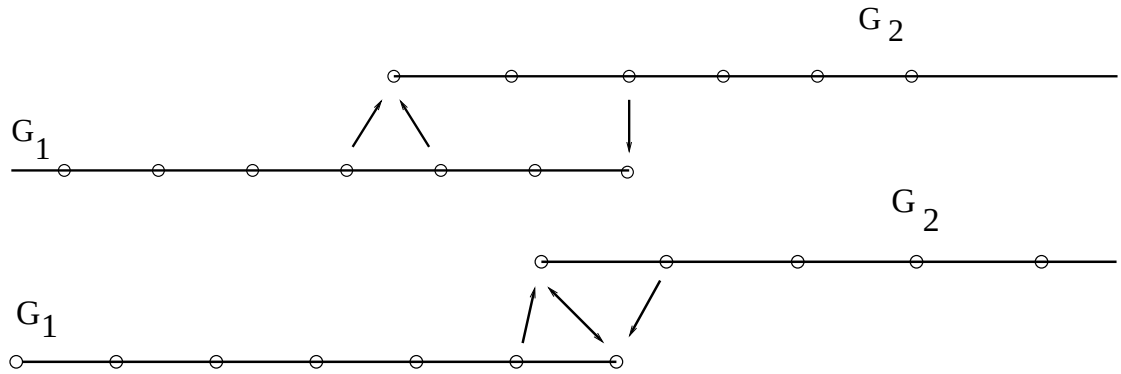

Figure 2: Interpolation between grids in one space dimension with one ghost point ($s=1$). Explicit (top) and implicit (bottom) interpolation.

are not allowed to be interpolation points. In implicit interpolation, interpolation points on one grid are allowed to be part of the interpolation stencil from the other grid. Implicit interpolation allows a smaller size overlap between the grids, but it is necessary to solve an algebraic system of equations for the interpolation values. Fig. 2 depicts explicit and implicit interpolation for a one dimensional example. In all test cases, explicit interpolation is used.

For a discretization with finite difference operators of stencil width $(2s+1)$ in one space dimension, the s first points on the grids (in regions of overlap) have to be interpolation points. No other boundary conditions except for interpolation are needed. In two and three space dimensions, there are s interpolation points in the direction normal to the interpolation boundary. We refer to this as s layers of interpolation points because the interpolation points form a layer that is s grid points thick, that follows the interpolation boundary. It would have been possible to use summation-by-parts boundary operators to decrease the number of interpolation points, but here we only use summation-by-parts operators at the real physical boundaries.

Overlapping grid generators such as Xcog [7] (two space dimensions) or Ogen [4] (three space dimensions), cut away underlying grids and determine which points need to be interpolated from other component grids. They output interpolation information in the form of a table. The user inputs the desired stencil width of the difference scheme and the desired width of the interpolation stencil. For example, three layers of interpolation points are needed with a sixth-order spatially central difference scheme.

We use Lagrangian interpolation between component grids. If the 3-D point (i,j,k) in grid g is interpolated from grid g_f with a stencil whose lower left corner is (i_f,j_f,k_f), and the location of (i,j,k) in the parameter space of g_f is (c_i,c_j,c_k), then the $(r+1)$th order interpolation formula is

$$u^{(g)}_{i,j,k}=\sum_{l=0}^{r}\sum_{m=0}^{r}\sum_{n=0}^{r}L_l(c_i)L_m(c_j)L_n(c_k)u^{(g_f)}_{i_f+l,j_f+m,k_f+n}, \tag{2.1}$$

where $u^{(g)}_{i,j,k}$ is the solution on grid g at grid point (i,j,k). The standard Lagrange polynomial basis is

$$L_l(\xi)=\prod_{\substack{p=0\\p\neq l}}^{r}\frac{\xi-x_{i_f+p}}{x_{i_f+l}-x_{i_f+p}},$$

for the i-direction and is similar for the j and k directions. (2.1) is used both when grid g is finer than grid g_f and when grid g is coarser than grid g_f. The Lagrange interpolation is defined in the parameter space of the grid mappings, and is therefore accurate for curvilinear grids under the assumption that the grid mapping used to generate the grid is smooth and well enough resolved.

The overlapping grid system enables us to use different numerical schemes on different component grids. The stencil width input to the grid generator is the maximum width over all discretizations that potentially will be used for any component grid. Higher order schemes require higher order interpolation between component grids. The interpolation stencil width, i.e., r in (2.1), in the overlapping grid system must be chosen to permit interpolation of high enough order.

3 Data structure and message passing

For parallel execution using message passing, we distribute each component grid evenly on the total number of processors available. This gives perfect load balancing, but the amount of communication is larger than optimal. However, because we use explicit time stepping, the communication cost is still only a small fraction of the total computation time. The approach is most efficient when the composite grid is made up of a few large component grids, because of low computation to communication ratio when component grids with very few grid points are distributed on a large number of processors.

Information about interpolation arrives from the grid generation program in a table with entry $(\mathbf{i},g,\mathbf{i}_f,g_f,\mathbf{c}_f)$ for each interpolation point. The meaning is that the point with index $\mathbf{i}$ in grid g, should interpolate from grid g_f, with an interpolation stencil that has point $\mathbf{i}_f$ as lower left corner and $\mathbf{c}_f$ as the location of point $\mathbf{i}$ in the curvilinear coordinate system g_f.

The whole interpolation table is read into each processor and split into one "get from" table representing interpolation points owned by the processor and one "give to" table representing values that need to be interpolated in the processor. The entries in the "get from" table are $(\mathbf{i},g,p)$, meaning that point $\mathbf{i}$ in grid g is an interpolation point that should get its value from processor p. The entries in the "give to" table are $(\mathbf{i}_f,g_f,\mathbf{c}_f,p)$, meaning that a value located at parameter values $\mathbf{c}_f$ in grid g_f should be interpolated with point $\mathbf{i}_f$ as lower left corner and then sent to processor p.

The "get from" and "give to" tables are built in the same order as the original non-parallel table. Therefore, if the interpolated values are sent in the order of the "give to" table from processor p they will be received in the right order in processor q. For

example, if the first entry in processor p "give to" table says that the interpolated value should be sent to processor q, then the first entry with processor p in the "get from" table in processor q is the corresponding point.

The tables are represented in such a way that all communication that is associated with the interpolation is done with a single call to the MPI function `MPI_Alltoallv`.

4 Governing equations and numerical method

The 3-D compressible Navier-Stokes equations considered in this study, written in non-dimensional form, are

$$\begin{aligned} &\rho_t + \operatorname{div}\rho\mathbf{u} = 0, \\ &(\rho\mathbf{u})_t + \operatorname{div}(\rho\mathbf{u}\mathbf{u}^T + pI) = \operatorname{div}\tau, \\ &e_t + \operatorname{div}\mathbf{u}(e+p) = \operatorname{div}(\tau\mathbf{u}) - \operatorname{div}\mathbf{q}. \end{aligned} \tag{4.1}$$

The dependent variables are the density, ρ, the velocity (column) vector $\mathbf{u}$, and the total energy e. Superscript T denotes tensor transpose, and I is the 3×3 identity tensor. p denotes the pressure and the 3×3 tensor D is the symmetric part of the velocity gradient tensor

$$D_{ij} = \frac{1}{2}\left(\frac{\partial u_i}{\partial x_j} + \frac{\partial u_j}{\partial x_i}\right).$$

The viscous tensor is given by

$$\tau = \frac{\alpha(T)}{Re}\left(-\frac{2}{3}\operatorname{div}\mathbf{u}I + 2D\right)$$

and the heat conduction vector is given by

$$\mathbf{q} = -\frac{\alpha(T)\gamma}{RePr(\gamma-1)}\nabla\frac{p}{\rho}.$$

Re denotes the Reynolds number, Pr is the Prandtl number, γ is the c_p to c_v ratio, and $\alpha(T)$ is the viscosity temperature dependency. The temperature is computed as

$$T = \frac{Mp}{R\rho}.$$

The constants M and R are the molar mass of the gas and the universal gas constant, respectively. In the computations a free stream state denoted by subscript ∞ is use to determine $M/R = T_\infty\rho_\infty/p_\infty$. For viscous computations Sutherland's law

$$\alpha(T) = \left(\frac{T}{T_\infty}\right)^{1.5}\frac{T_\infty+110}{T+110}.$$

is used. For inviscid computations, $\alpha(T) = 0$. Note that the overlapping grid method described above is also applicable for the magnetohydrodynamics (MHD) equations.

For flows containing steady or nearly steady strong shocks on parts of the flow field, and unsteady turbulence with shocklets on other parts of the flow field, we propose to employ variable order multiblock overlapping grid methods with different schemes on different blocks. The recently developed low dissipative high order filter schemes [9, 11] are considered for regions of smooth flows and for regions that require high order of accuracy. For regions with strong steady shocks, second-order shock-capturing schemes are employed. The low dissipative high order filter scheme [11] consist of two steps, a full time step using a spatially high order non-dissipative (or very low dissipative) base scheme, followed by an adaptive multistep filter consisting of the products of wavelet based flow sensors and linear and nonlinear numerical dissipations to filter the solution [9]. The numerical dissipation control idea is very general and can be used in conjunction with spectral, spectral element, finite volume and finite difference spatial base schemes. The type of shock-capturing scheme used as nonlinear dissipation is very general and can be any dissipative portion of the high resolution TVD, MUSCL, ENO, or WENO shock-capturing methods. The shock-capturing dissipations usually contain flux limiters. The linear filter can be the standard spectral or compact filter, or the product of a high order linear dissipation and an appropriate flow sensor. By design, the flow sensors, spatial base schemes and linear and nonlinear dissipation models are stand alone modules. Therefore, a whole class of low dissipative high order filter schemes can be derived at ease. Extensive numerical testing on the filter schemes using finite difference approach and single block grids have been conducted [11]. These numerical experiments include high order central spatial base schemes of order up to 10, adaptive nonlinear filters of order up to 9 and adaptive linear filter of order up to 12. It was found that for certain multicale flows, multiblock grids are necessary if adaptive grids are not used.

5 Numerical tests

Before embarking on multiscale problems containing mixed steady and unsteady shock/turbulence interaction, we first illustrate several simple blunt body test cases to validate the high order overlapping approach. The test cases were intentionally chosen to contain strong steady bow shock without mixed unsteady components in the flow. Furthermore, in order to validate the proposed variable high order multiblock overlapping grid methods, as an illustration, only two different orders of schemes are used. On some component grids, the viscous and inviscid flux derivatives (4.1) are discretized by sixth-order central finite difference spatial base schemes with summation-by-parts boundary modification of the difference operators [5]. A small amount of eighth-order numerical dissipation is needed to stabilize the scheme if filters are not used. See [11] for a discussion. On other component grids, the convective terms in (4.1) are discretized by a second-order TVD type scheme with the minmod limiter, and the viscous flux deriva-

tives are discretized by a second-order central scheme. When the spatial discretizations are mixed with TVD spatial schemes on some component grids and sixth-order spatial schemes on other component grids, the classical fourth-order Runge-Kutta temporal discretization is used on all grids. The linear and nonlinear filter steps described in [11] are not necessary. In the presence of the multiscale unsteady shock/turbulence portion of flows, the filter steps are needed for the improvement of accuracy and stability.

In most of the considered test cases the flow consists of a major steady bow shock and smooth flow on the rest of the computational region. Unlike the standard time-marching to the steady state, in order to access the capability of unsteady computations, the computations are time accurate.

The overlapping grid generator Xcog [7] is used to generate the two-dimensional overlapping grids, and the Ogen grid generator [4] is used to generate the three-dimensional overlapping grids. The grids were generated with an overlap that allows evaluation of nine-point stencils, required for the eighth-order numerical dissipation term used in the sixth-order spatial base scheme. Unless otherwise stated, the width of the interpolation stencil is five points, which means the interpolation is fifth-order accurate. Errors from interpolation can reduce the convergence order of the sixth-order scheme, but as we will see below the errors in the computed solutions are reduced even more than what can be explained by the interpolation. Other effects will dominate the error. The interpolation is explicit in all computations.

5.1 Accuracy of an inviscid flow: Errors from a bow shock

The first test case is to illustrate improvement in accuracy when switching to a high order centered scheme on component grids that do not have any steady strong shocks. This test case is an inviscid flow with free stream Mach number 3 past a cylinder with radius 0.5 and $\gamma = 1.4$. It is well known that the presence of a shock can reduce the actual convergence rate to first order as the grid is refined, even when using a numerical method of formally high order of accuracy [3]. Here, this effect in the context of high order methods with SBP boundary conditions as described in [11] is studied.

The flow in the wake region depends strongly on the viscosity, thus, we do not consider the wake for this inviscid computation. The two overlapping grids are shown in Fig. 3. A second-order TVD scheme is used on the grid at the shock, whereas, a sixth-order central spatial scheme is used on the grid around the cylinder. For comparison, a second-order TVD scheme on both grids is used. In addition, we will compare three different grid refinements with the coarsest overlapping grid having 81×43 (cylinder) and 155×55 (shock) points. The next finer grid has 161×85 and 301×109 points, and the finest grid has 321×169 and 601×217 points. Results on these three overlapping grid systems are labeled by h, $h/2$, and $h/4$ in Fig. 4.

For inviscid flows, the entropy is constant on the streamlines, with possible jumps at the shocks. With knowledge of the free stream state, we can compute analytically, by the Rankine-Hugoniot conditions, the entropy on the streamline that coincides with $y=0$ in

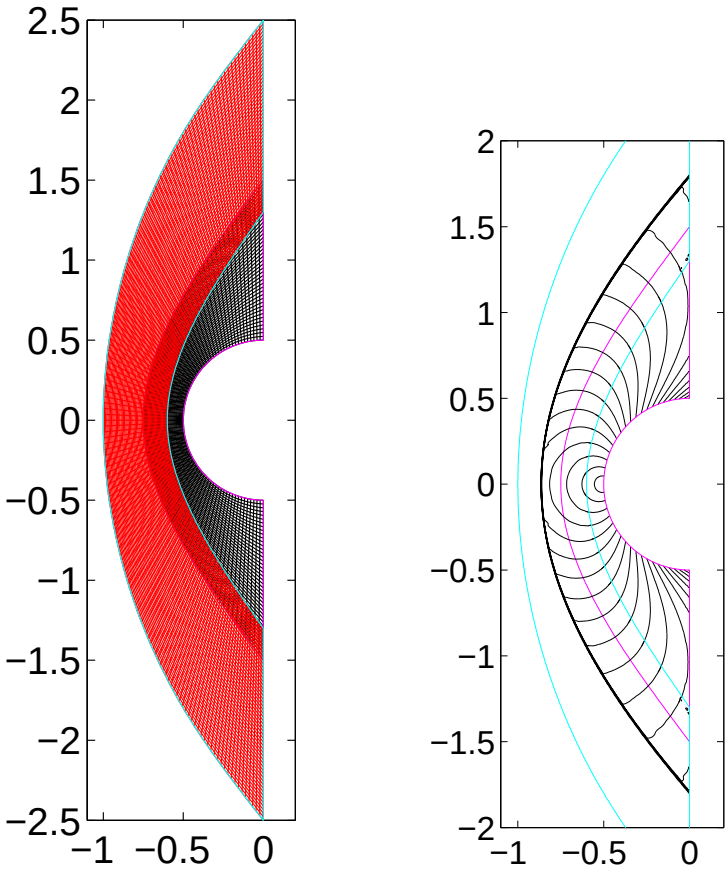

Figure 3: Two overlapping grids for inviscid computation (left). Computed flow field at free stream Mach number 3 (right).

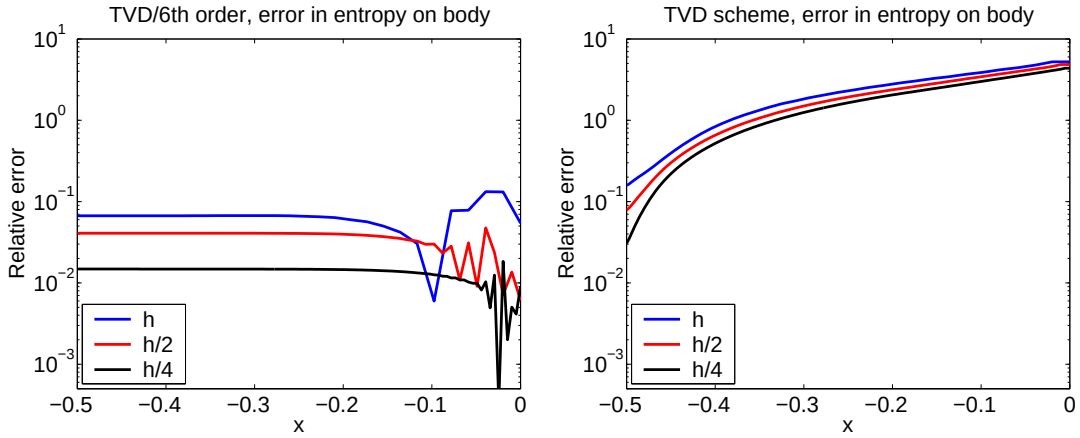

Figure 4: Relative error in entropy on cylinder as a function of x. Mixed second-order TVD and sixth-order (left) and second-order TVD on both grids (right). (81×43,155×55) grid points (blue), (161×85, 301×109) grid points (red), and (321×169, 601×217) grid points (black).

the free stream. This streamline passes normally through the bow shock, and attaches to the body of the cylinder. The error in entropy along the body will be used as a measure of accuracy.

The left subplot in Fig. 4 displays the relative entropy error along the streamline for inviscid flow with a second-order TVD scheme at the shock grid and the sixth-order centered spatial scheme on the remaining component grid. The right plot of Fig. 4 shows the same error for a computation with a TVD difference scheme on both component grids. Fig. 4 shows that the error decreases with a first-order accurate convergence rate for the sixth-order scheme. This is most likely due to errors that originate at the bow shock, [3]. The behavior of the error with time is that a quasi steady state is reached around the dimensionless time 10, where the error is considerably smaller than the steady state errors shown in Fig. 4. The error then increases to the level shown in Fig. 4 where a steady state seems to have been reached. Nevertheless, the error with the mixed TVD/sixth-order computation is in absolute terms much smaller than the error from using only the TVD difference scheme, shown in the right subplot of Fig. 4.

The computations with the TVD scheme on all component grids in Fig. 4 were made with third-order interpolation between the component grids. Because it is the error on the boundary we are plotting, the wall boundary conditions used will also affect the error. The poor convergence in the right subplot of Fig. 4 is probably caused by the first-order accurate wall boundary conditions used. For the sixth-order scheme, the SBP boundary operator reduces the order on the boundary to third. We conclude that mixing a high order method with a second-order TVD scheme gives a smaller error than obtained with only the second-order TVD difference scheme on both grids, but that the high order convergence rate is not obtained.

5.2 Accuracy of a viscous flow based on the skin friction coefficient

The same test case considered previously is considered when physical viscosity is added. Here, we illustrate a computation for a Reynolds number 500 flow past a cylinder with radius 0.5. The Prandtl number is 0.72, γ is 1.4, and $T_\infty = 273.15K$. Studies also were performed for Reynolds numbers 500,1000,2000 and 10,000. The size of the tail in the wake region depends on the Reynolds number.

We compare solutions on three different set of composite grids, Coarse, Medium, and Fine. The domain is discretized by the overlapping grid configuration displayed in Fig. 5. Each component grid system consists of four grids, a base grid that covers the entire domain, a curved grid around the bow shock, a fine polar grid near the cylinder surface, and a fine grid that covers the wake region.

Table 1 gives the number of grid points in these grids. The thickness of the cylinder grid in the radial direction is 0.1, the number of grid points are chosen such that the grid spacing is of similar size radially and tangentially. The size of the wake grid is such that the grid spacing is of similar size as the spacing of the cylinder grid. The finest grid has discretization step $h = 1.7 \times 10^{-3}$ in the radial direction, which gives 26 grid points over

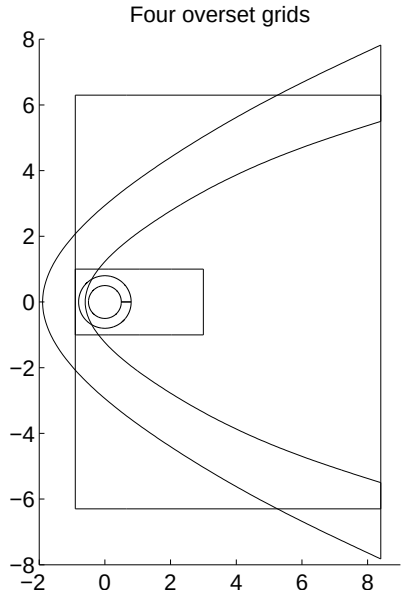

Figure 5: Overlapping grid domains used for computations with body fitted grids.

Table 1: Number of grid points in composite grids for the three computations. The body grid and the wake grid have cell aspect ratios close to one.

	Coarse	Medium	Fine
base grid	100×136	200×272	200×272
wake grid	400×200	800×400	1200×600
shock grid	160×35	320×70	320×70
body grid	352×15	697×30	1387×60

the width $1/\sqrt{Re}$ for Reynolds number 500.

Fig. 6 shows local Mach number contours of a solution computed on the Medium grid. The grid boundaries are outlined in color (or gray). The close up to the right shows good agreement of the contour lines between the component grids. The structure in the wake and the trailing discontinuities can be completely resolved by the centered scheme and the physical viscosity. No numerical dissipation is needed. This is not the case for the bow shock, which is unresolved even on the finest grid. To assess the accuracy of the computations, we plot the skin friction coefficient along the body,

$$C_f = \frac{\alpha(T)}{Re} \frac{1}{\frac{1}{2}\rho_\infty U_\infty^2} \frac{\partial V}{\partial n}, \tag{5.1}$$

where V denotes the velocity tangential to the boundary.

Fig. 7 shows the skin friction coefficient on the three different grids. The left subplot uses a sixth-order spatial scheme on all grids except on the grid around the bow shock,

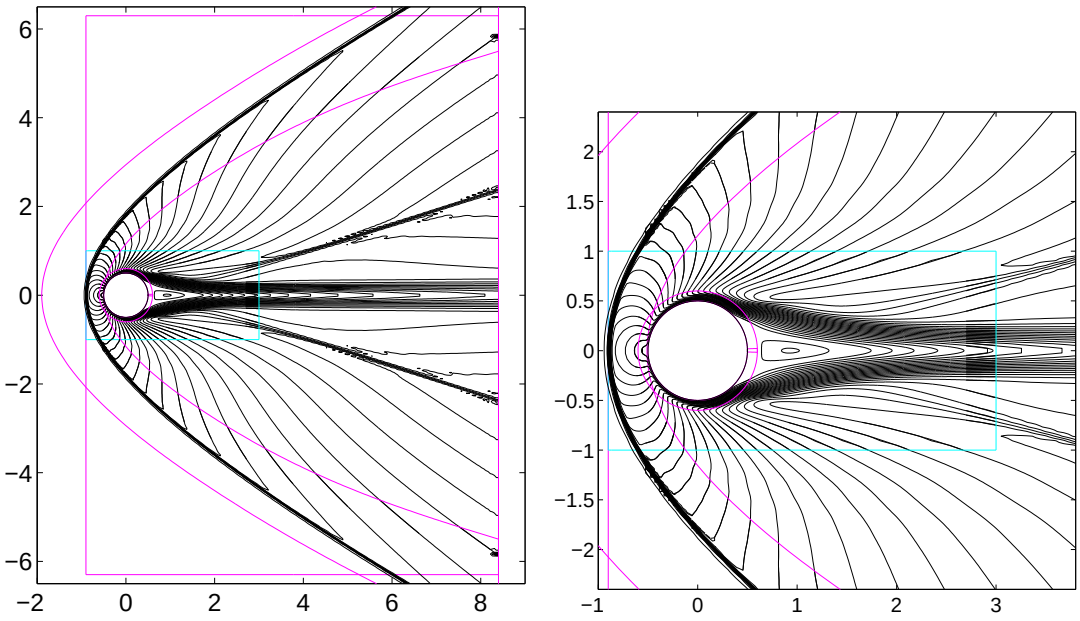

Figure 6: Solution on overlapping grids for free stream Mach number of 3 and $Re_\infty = 500$. Mach number contours. Sixth-order spatial scheme on all grids except the bow shock grid. Close up of the region near the cylinder (right).

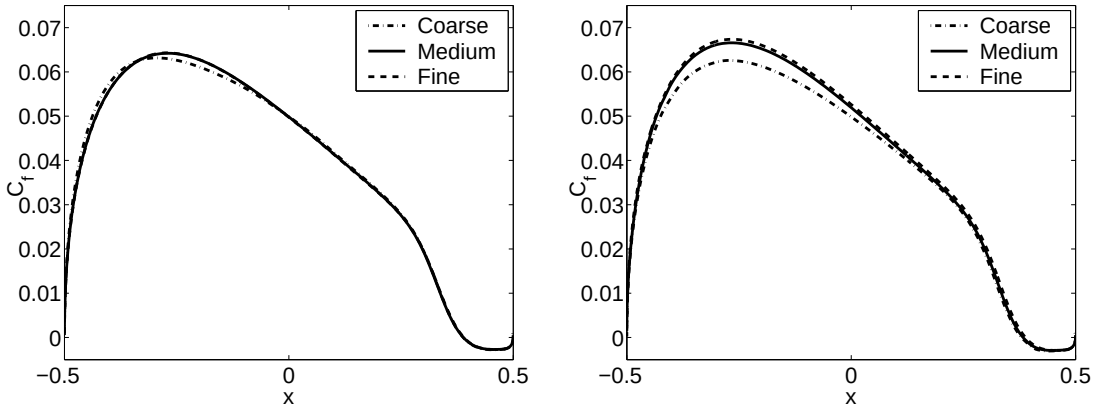

Figure 7: C_f as function of x along the cylinder surface. Three overlapping grids of increasing refinement. Sixth-order spatial scheme on all grids except the bow shock grid (left), and TVD scheme on all four grids (right).

where a second-order TVD scheme is used. The right subplot shows C_f for the same computations, but with the TVD difference scheme on all grids. It is clearly seen that the mixed sixth-order/TVD method converges faster than the pure TVD method, and yet both methods required a similar CPU time. From this we infer that the errors on the body are not completely dominated by the errors originating from the bow shock grid, because improvement can be made by switching from TVD to sixth-order near the body.

5.3 A 3-D space vehicle example

We first study the inviscid flow past an Apollo-like re-entry space vehicle. The flow conditions are the same as used for the Apollo Fire II experiment configuration [8]. The free stream Mach number is 16, the free stream temperature is $237K$, and the angle of attack is zero degrees. The geometry with overlapping grid system is outlined in Fig. 8. There are six grids in total. The Cartesian background grid in blue color has a fairly coarse grid spacing. The body is defined by a spline curve, rotated around the x-axis (magenta) with two orthographic cap grids (light blue and dark blue) that cover the polar singularities. A cylindrical grid (green) together with a Cartesian grid (red) that covers its polar singularity are inserted in the wake region. The grid spacing is approximately 0.05 on the body and wake grids and about five times larger on the Cartesian background grid. The number of points is $88\times81\times81$ for the base grid, $160\times43\times130$ for the cylinder grid in the wake, $101\times23\times23$ Cartesian grid in the wake to cover the cylinder grid singularity, $221\times255\times17$ near the body of Apollo capsule, $65\times65\times17$ at the cap, forward end covering body grid singularity, $53\times53\times17$ at the cap, rear end (at wake) covering body grid singularity. Computed inviscid solutions using the mixed sixth-order/TVD scheme indicate a smooth transition among all overlapping regions (figures are not shown due to page limitation).

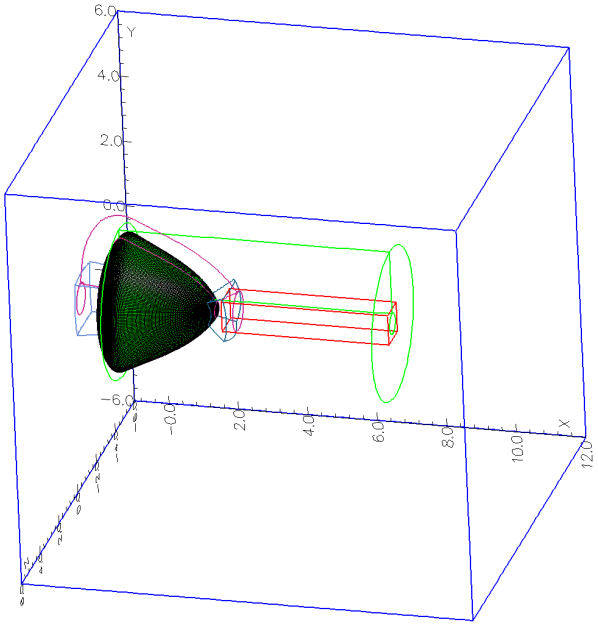

Figure 8: Overlapping grid system for re-entry vehicle computation.

As a preliminary 3-D viscous flow computation, a computed flow field on the same overlapping grid configuration in Fig. 8 for the viscous case with Reynolds number of 500 is shown in Fig. 9. Due to the narrow overlapping regions of this grid system, we are

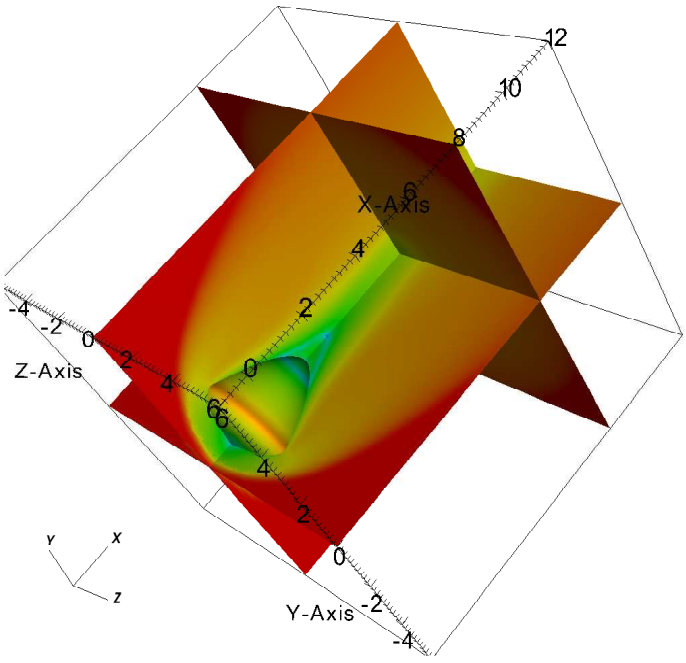

Figure 9: Mach number color levels, logarithmic scale. The free stream Mach number is 16 and the Reynolds number is 500.

limited to the second-order TVD scheme for the convection terms and second-order spatial scheme for the diffusion terms. Direct numerical simulation (DNS) test cases using finer grids and high order filter schemes near the shoulder and wake regions are work in progress and will be reported in future publications.

In all of the 2-D and 3-D test cases, the computed flow solution indicates a smooth transition from one component grid to the other. The above 3-D result serves as a validation of the variable order overlapping grid methods for 3-D flows.

6 Conclusions

We have described an extension of our previously developed high order schemes for single block grid to geometries discretized by overlapping grids. The 2-D and 3-D test cases illustrate the computations where high order schemes are used on some of the component grids, and shock-capturing schemes are used on other component grids. Examples have shown that the overall error in high speed flow computations is smaller when high order schemes are used on some component grids. This is expected but not completely trivial because first order errors that propagate from shocks, or other lower order errors from grids where lower order methods are applied, could potentially make high order methods with zero gain for multiblock variable order of accuracy discretizations.

Many questions regarding error propagation for shock problems remain to be answered. Future plans include a more extensive study of such phenomena in practical settings. The 3-D re-entry space vehicle computations will be extended with the objective to study the flow, and how the flow is affected by the order of accuracy of the scheme in the shoulder and wake region for moderate and high Reynolds numbers with non-zero angles of attack.

Acknowledgments

This work performed under the auspices of the U.S. Department of Energy by Lawrence Livermore National Laboratory under Contract DE-AC52-07NA27344.

We thank Bill Henshaw at Lawrence Livermore National Laboratory for his assistance with the Ogen grid generator. The financial support from the NASA Fundamental Aeronautics (Hypersonic) program for the second author is gratefully acknowledged. Partial support from the SciDAC/DOE grant for the first author is also gratefully acknowledged.

References

[1] J. A. Benek, P. G. Buning, and J. L. Steger. A 3-D Chimera grid embedding technique. *AIAA paper 85-1523*, pages 322–331, 1985.

[2] G. Chesshire and W.D. Henshaw. Composite overlapping meshes for the solution of partial differential equations. *J. Comput. Phys.*, 90(1):1–64, 1990.

[3] B. Engquist and B. Sjögreen. The convergence rate of finite difference schemes in the presence of shocks. *SIAM J. Numer. Anal.*, 35:2464–2485, 1998.

[4] W.D. Henshaw. Ogen: An overlapping grid generator for Overture. Research Report UCRL-MA-132237, Lawrence Livermore National Laboratory, 1998.

[5] P. Olsson. Summation by parts, projections and stability, I. *Math. Comp.*, 64:1035–1065, 1995.

[6] E. Pärt-Enander and B. Sjögreen. Conservative and non-conservative interpolation between overlapping grids for finite volume solutions of hyperbolic problems. *Computers Fluids*, 23:551–574, 1994.

[7] N. A. Petersson. An algorithm for assembling overlapping grid systems. *SIAM J. Sci. Comput.*, 20(6):1995–2022, 1999.

[8] K. Sinha, M. Barnhardt, and G. V. Candler. Detatched eddy simulation of hypersonic base flows with application to Fire II experiments. Paper 2004-2633, AIAA, June 2004. 34th AIAA Fluid Dynamics Conference and Exhibit, Portland, Oregon.

[9] B. Sjögreen and H. C. Yee. Multiresolution wavelet based adaptive numerical dissipation control for shock-turbulence computation. *J. Sci. Comput.*, 20:211–255, 2004.

[10] M. Vinokur and H. C. Yee. Extension of efficient low dissipative high order schemes for 3-D curvilinear moving grids. NASA Technical Memorandum 209598, NASA Ames Research Center, June 2000.

[11] H. C. Yee and B. Sjögreen. Development of low dissipative high order filter schemes for multiscale Navier-Stokes/MHD systems. *J. Comput. Phys.*, 225:910–934, 2007.